NANOMATERIALS

Wafer-scale single-crystal hexagonal boron nitride film via self-collimated grain formation

Joo Song Lee[1,2], Soo Ho Choi[3], Seok Joon Yun[4], Yong In Kim[5], Stephen Boandoh[6], Ji-Hoon Park[4,5], Bong Gyu Shin[4,7,8], Hayoung Ko[1,5], Seung Hee Lee[2], Young-Min Kim[4,5], Young Hee Lee[4,5]*, Ki Kang Kim[6]*, Soo Min Kim[1]*

Although polycrystalline hexagonal boron nitride (PC-hBN) has been realized, defects and grain boundaries still cause charge scatterings and trap sites, impeding high-performance electronics. Here, we report a method of synthesizing wafer-scale single-crystalline hBN (SC-hBN) monolayer films by chemical vapor deposition. The limited solubility of boron (B) and nitrogen (N) atoms in liquid gold promotes high diffusion of adatoms on the surface of liquid at high temperature to provoke the circular hBN grains. These further evolve into closely packed unimodal grains by means of self-collimation of B and N edges inherited by electrostatic interaction between grains, eventually forming an SC-hBN film on a wafer scale. This SC-hBN film also allows for the synthesis of wafer-scale graphene/hBN heterostructure and single-crystalline tungsten disulfide.

Hexagonal boron nitride (hBN), called white graphite, consists of atomically flat layers of alternating hexagonal B and N atoms held together by van der Waals interaction between layers. The insulating hBN plays a role in a variety of fundamental science and technology fields, serving, for example, as a platform for charge fluctuation, contact resistance, gate dielectric, passivation layer, Coulomb drag, and atomic tunneling layer (*1*–*6*). Although micrometer-sized hBN grains have been commonly employed for fundamental studies, wafer-scale single-crystalline hBN (SC-hBN) films are not yet available for practical applications. One approach to reach SC-hBN film is to start with grains of a triangular shape at random orientations and eventually merge them to form the polycrystalline hBN (PC-hBN) film. However, grain boundaries between randomly oriented hBN grains inevitably yield PC-hBN film. An alternative to achieve SC-hBN film is therefore desired.

The concept for the synthesis of SC-hBN film is schematically shown in Fig. 1, A to C. Au is liquefied at high temperatures (~1100°C) and robustly anchored on W foil still holding in solid state owing to the high melting temperature (~3422°C). The key idea is to retain a flat liquid Au with high surface tension to allow for strong adhesion to borazine precursors (Fig. 1A, i). The solubility of B and N atoms in liquid Au (at 1100°C) is ~0.5 and ~0 atomic %, respectively (*7*, *8*), ensuring prevalent surface diffusion of B and N atoms rather than bulk diffusion (Fig. 1A, ii). At the initial growth stage (~30 s), the diameter sizes of circular hBN grains are irregularly distributed from approximately a few micrometers to ~14.0 μm (Fig. 1C, i, and supplementary materials and methods). The circular hBN grains increase to a regular size of 14.5 μm after 10 min of growth (Fig. 1C, ii). These circular hBN grains are also observed on liquid Cu substrate at high temperatures, rather than triangular hBN grains on solid substrates at low temperatures (*9*–*12*). The detailed edge structures and the corresponding edge energy of circular hBN grains should be investigated further. High diffusion of adatoms on a smooth liquid surface at high temperatures provokes the circular hBN domains. The size and uniformity of hBN grains are strongly influenced by the content of borazine and H_2 (fig. S1).

After a prolonged growth of 20 min (Fig. 1C, iii), the density of hBN grains further increases without a noticeable progressive change in size. Moreover, the well-regulated sizes of hBN grains are linearly aligned in some regions, indicated by white arrows. When two hBN grains merge, the individual grains are rotated by less than 60° with respect to each other by means of attractive Coulomb interaction between B (Lewis acid) and N (Lewis base) atoms, leading to a seamless stitching by the self-collimated hBN grains (Fig. 1A, iii and iv, and fig. S2), which is as a result of the cohesive energy of a B–N bond being much higher than that of an N–N or B–B bond at a high growth temperature (1100°C) (fig. S3). In addition, the orientation of the hBN grains is not commensurate with the lattice orientation of the underlying Au substrate, which is confirmed by electron backscatter diffraction measurements (fig. S4). The hBN grains are transformed further into a hexagonal close-packed structure at 30-min growth time through the self-collimation of hBN grains (Fig. 1C, iv). The seamless stitching of aligned hBN grains with the absence of grain boundary was further confirmed by the statistical analysis of a series of selected-area electron diffraction (SAED) patterns in transmission electron microscopy (TEM) by means of hBN transfer on a graphene-supported (or MoS_2-supported) TEM grid (figs. S5 to S8). Even at a longer growth time (~90 min), hBN grains were not fully merged with the presence of nanopores observed at a fixed precursor flow rate (fig. S9). We were able to achieve the full coverage of wafer-scale hBN film through two-step growth of elevated growth time and additional precursor flow rate (Fig. 1A, vi, and Fig. 1C, v to vi, and supplementary materials and methods). A wafer-scale full SC-hBN film is obtained with a size of 3 cm by 3 cm, followed by transfer to an SiO_2/Si wafer (Fig. 1B).

The grain size distribution and coverage as a function of growth time are displayed in Fig. 1D. The grain size rapidly increases to saturate at ~14.5 μm within 5-min growth time, whereas the standard deviation of the grain size abruptly decreases. The hBN grains are rapidly grown at a rate of ~283 μm^2/s owing to the high-temperature process (1100°C), which is ~10^6 times higher than the typical growth rate of hBN on solid substrate at lower temperature (~1000°C) (*10*). Meanwhile, the hBN coverage gradually increases and saturates to a full coverage at 60-min growth time. We emphasize that monolayer SC-hBN is achieved on a wafer scale with no appreciable multilayer hBN islands, confirmed by scanning electron microscope (SEM) images (fig. S10). This implies that monolayer hBN film is grown exclusively by means of surface-mediated growth on catalytic metal substrate under the current growth conditions. The stoichiometry of B and N atoms is 1:1.03, confirmed by x-ray photoelectron spectroscopy (XPS) (fig. S11). Furthermore, the expensive Au foil can be reused for the repeated growth of SC-hBN film (fig. S12).

We characterized the single crystallinity of hBN film on a large scale by three different methods: electron diffraction in TEM, liquid crystal (LC)–assisted polarized optical microscope (POM), and low-energy electron diffraction (LEED). The monolayer nature of hBN film is identified at the edge of hBN grains prepared on a TEM grid (Fig. 2, A and B), again confirming the results of atomic force microscopy analysis (fig. S13). Furthermore, the high-resolution TEM displays clear hexagonal B and N atoms (Fig. 2C). Fast Fourier transform spots from the

[1]Institute of Advanced Composite Materials, Korea Institute of Science and Technology (KIST), Wanju-Gun, 55324, Republic of Korea. [2]Applied Materials Institute for BIN Convergence, Department of BIN Fusion Technology and Department of Polymer-Nano Science and Technology, Chonbuk National University, Jeonju, 54896, Republic of Korea. [3]Department of Physics, Dongguk University-Seoul, Seoul, 04620, Republic of Korea. [4]Center for Integrated Nanostructure Physics (CINAP), Institute for Basic Science (IBS), 16419, Republic of Korea. [5]Department of Energy Science, Sungkyunkwan University, Suwon, 16419, Republic of Korea. [6]Department of Energy and Materials Engineering, Dongguk University-Seoul, Seoul, 04620, Republic of Korea. [7]Center for Quantum Nanoscience (QNS), Institute for Basic Science (IBS), Ewha Womans University, Seoul, 03760, Republic of Korea. [8]Department of Physics, Sungkyunkwan University, Suwon, 16419, Republic of Korea.
*Corresponding author. Email: kkkim@dongguk.edu (K.K.K.); leeyoung@skku.edu (Y.H.L.); smkim@kist.re.kr (S.M.K.)

whole image (inset of Fig. 2C) demonstrate only one set of hexagonal spots, assuring the hexagonal structure of the sample. The d-spacings of the $(10\bar{1}0)$ and $(11\bar{2}0)$ planes are 2.17 and 1.26 Å, respectively, confirming SC-hBN, in good agreement with reported values (*13*). The aberration-corrected dark field in the scanning tunneling electron microscopy image and intensity profile along the white-dashed line clearly distinguish the B and N atoms in the hexagonal lattice, with higher intensity of N atoms than that of B atoms (Fig. 2, D and E) (*14*, *15*). The bond length between B and N atoms is 1.45 Å (*16*). A series of SAED patterns vertically stacked by nine frames from regions I to IX in Fig. 2A (fig. S14) exhibit identical six hexagonal dots (Fig. 2F), ensuring that the hBN film is single crystalline in a selected area of ~300 μm by 300 μm. By spin-coating nematic LC on hBN film, the POM patterns in the absence of grains are not altered, regardless of polarized angles, again demonstrating the single crystallinity of hBN on a large scale (Fig. 2G and fig. S15). This is contrasted with inhomogeneous grain speckles with polarized angles due to the presence of multi-hBN grains in the PC-hBN film (fig. S16) (*17*). LEED images from 16 different regions in a 4 mm by 4 mm area with a separation of 1 mm display identical distorted hexagonal spots with the same rotation angle (Fig. 2H), indicating that the hBN film is indeed a single crystal over the whole area. An elongated uniaxial strain of ~14% is observed, similar to that noted in previous reports (*18*–*20*). The hBN lattice is relaxed after hBN transfer on the TEM grid and, consequently, the regular hexagonal lattice is preserved by restoring the strain without provoking fracture.

Our SC-hBN film can serve as a platform growth substrate for construction of a vertical, two-dimensional (2D) heterostructure or single-crystal 2D material on a wafer scale (*21*). We now demonstrate the synthesis of a single-crystal vertical graphene/hBN heterostructure (SC/Gr-hBN) and single-crystal WS_2 (SC-WS_2) film on a wafer scale. Epitaxial graphene is successively grown in situ on SC-hBN film at 1100°C under methane atmosphere (Fig. 3A and supplementary materials and methods). The orientationally aligned hexagonal graphene domains on SC-hBN film are clearly visible (Fig. 3B), eventually achieving the monolayer graphene film in a large area at a prolonged growth time while preserving SC-hBN film (Fig. 3C). SC-Gr/hBN film is transferred onto the SiO_2-Si substrate and onto the TEM grid for further characterizations. The G-band (~1585 cm^{-1}) and 2D-band (~2686 cm^{-1}) peaks in the Raman spectrum are clearly detected without a noticeable D-band (~1330 cm^{-1}) (Fig. 3D). Moreover, the E_{2g} phonon mode of monolayer hBN film is observed near 1370 cm^{-1} (inset of Fig. 3D). The SC-Gr/hBN film stacked at eight different regions in SAED patterns in TEM (fig. S17) shows an identical set of six hexagonal dots (Fig. 3E). This proves that the well-defined structure between graphene and SC-hBN is constructed by means of AA′-stacking with two distinct dots assigned to the $(10\bar{1}0)$ planes of graphene and hBN (inset of Fig. 3E) and the relative rotation angle between two dots of 0.64 ± 0.34° obtained from eight different regions (fig. S17). Furthermore, the moiré pattern of Gr/hBN heterostructure is clearly observed with a wavelength of ~9.20 nm rotated by 1.2° (Fig. 3, F and G, and fig. S18), ensuring the successful synthesis of SC-Gr/hBN film through van der Waals epitaxy (*22*). The distinct B-K, C-K, and N-K edges in the electron energy loss spectroscopy with preserved stoichiometry of B and N of 1.03:1 further support the growth of SC-Gr/hBN film (fig. S18C).

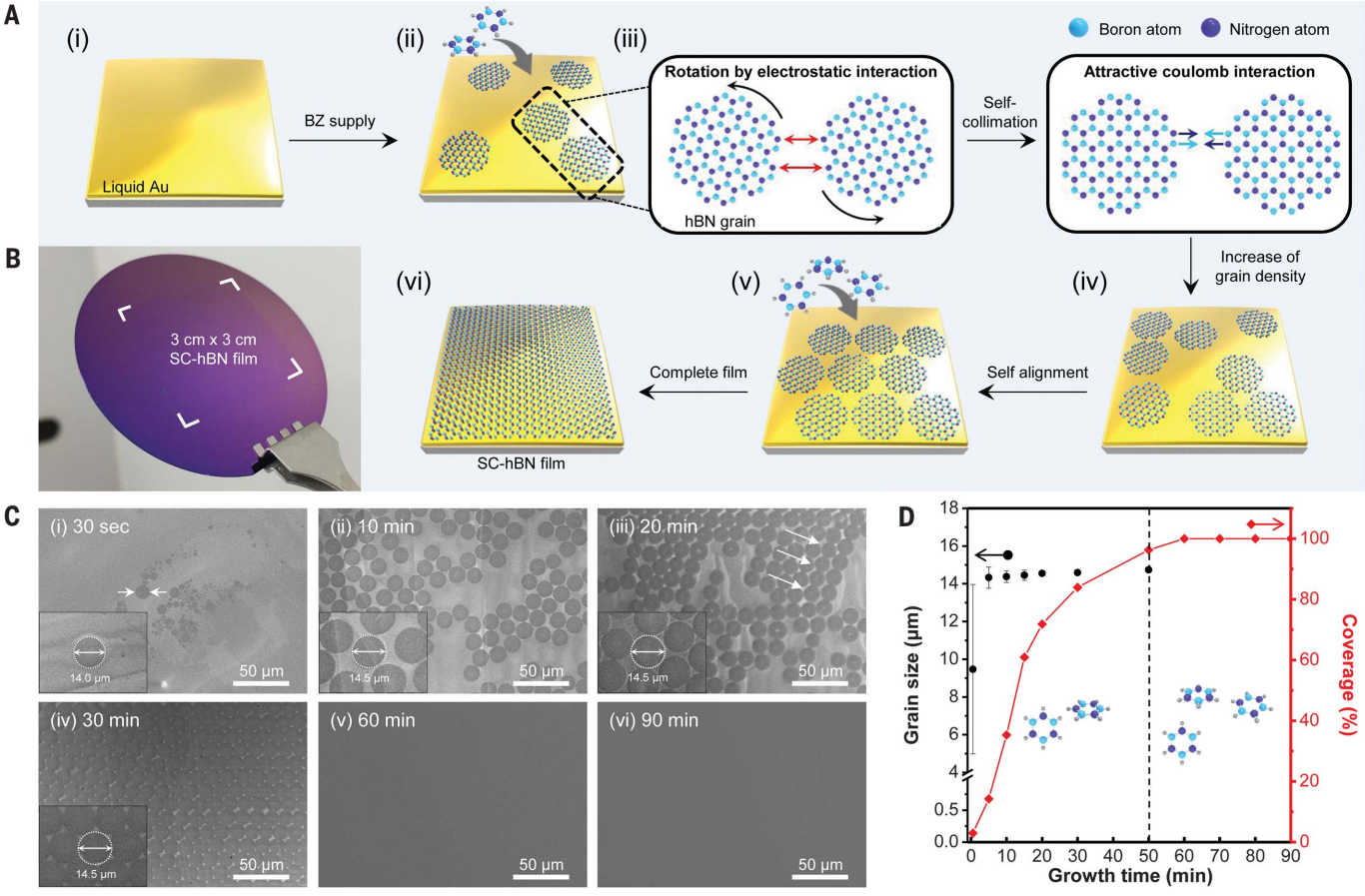

Fig. 1. Synthesis of single-crystal hBN film. (**A**) Schematic illustration for the growth of SC-hBN film by means of self-collimated circular hBN grains with a rotation invoked by the attractive Coulomb interaction of B and N edges between grains (i to vi). BZ, borazine. (**B**) Photograph of a wafer-scale SC-hBN film on a SiO_2-Si wafer. (**C**) Growth evolution of SEM images of hBN film. Single-headed arrows indicate linear alignment of hBN grains. (**D**) Time evolution of hBN grain size and coverage. Full coverage of monolayer hBN film is achieved at 60-min growth time. Error bars indicate the size deviation of hBN grains.

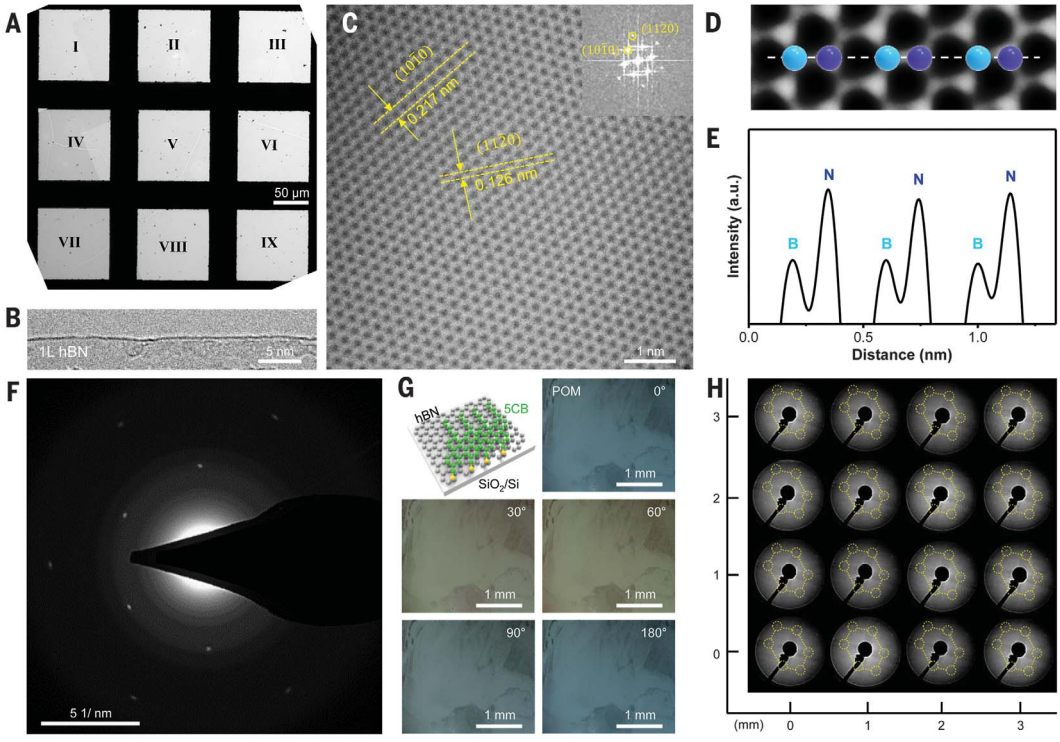

Fig. 2. Atomic structures of SC-hBN film. (**A**) TEM image of SC-hBN film transferred onto TEM grid divided into nine regions. (**B**) The folded edge of a monolayer (1L) SC-hBN film. (**C**) High-resolution TEM image of SC-hBN film. The inset shows the fast Fourier transform of the whole image. The d-spacings of (10$\bar{1}$0) and (11$\bar{2}$0) planes of hBN are 0.217 and 0.126 nm, respectively. (**D**) Aberration-corrected dark-field TEM image of SC-hBN film. Cyan and blue balls indicate B and N atoms, respectively. (**E**) Intensity profile along white-dashed line in (D). a.u., arbitrary units. (**F**) Vertically stacked SAED pattern image of nine segments from regions I to IX in (A). (**G**) Schematic illustration of aligned LC (5CB) on SC-hBN and optical images of 5CB-coated SC-BN film as a function of the polarized light angles: 0, 30, 60, 90, and 180°. (**H**) LEED pattern images of SC-hBN film on Au substrate over an area of 4 mm by 4 mm.

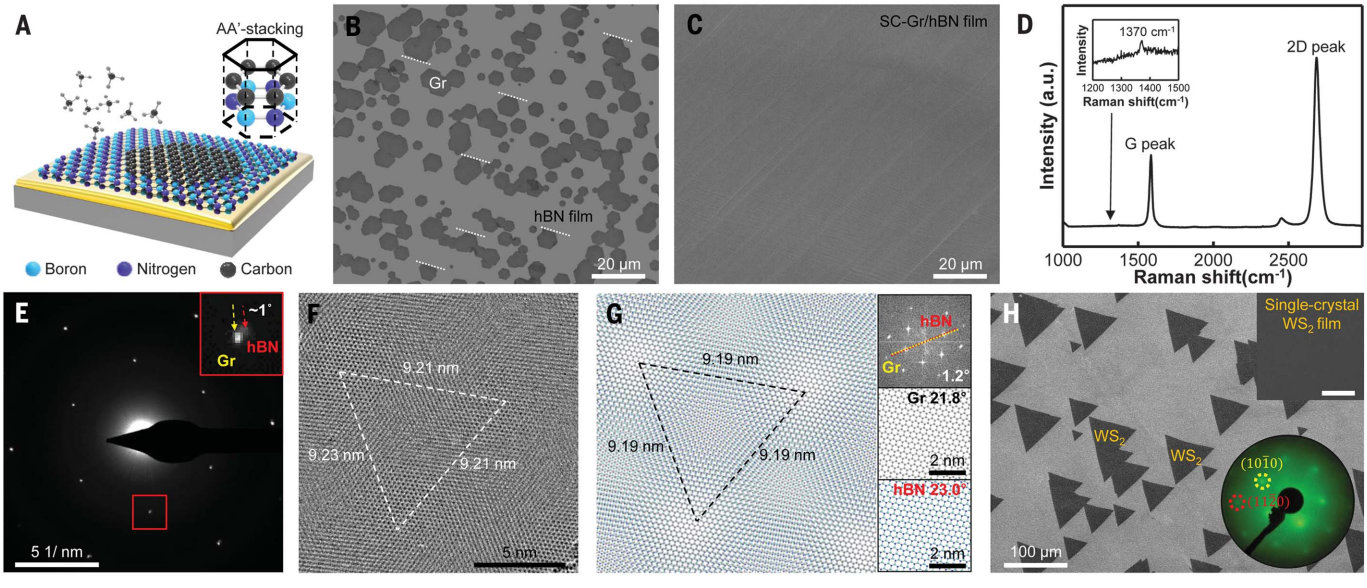

Fig. 3. Direct growth of vertical SC-Gr/hBN heterostructure and single-crystal WS_2 film. (**A**) Schematic for the direct growth of commensurate epitaxial graphene on SC-hBN film. (**B**) SEM image of as-grown hexagonal graphene domains on SC-Gr-BN film and (**C**) the corresponding large-area SC-Gr/hBN film. The dashed lines in (B) indicate the aligned orientation of individual hexagons. (**D**) Representative Raman spectrum of graphene/hBN heterostructure after transfer onto SiO_2/Si substrate. The inset shows the Raman spectrum near 1370 cm^{-1}, assigned to the E^1_{2g} phonon mode of hBN. (**E**) Combined SAED pattern stacked vertically by eight SAED patterns for graphene/hBN heterostructure. The inset shows a zoomed-in SAED pattern of one of the hexagonal spots, revealing an angle deviation of ~1° between two spots. (**F**) Representative moiré pattern of graphene on hBN, with a rotation angle of ~1.2° between the components, and (**G**) the corresponding simulated moiré pattern. The wavelength of the moiré pattern is ~9.20 nm. The three insets depict the diffraction pattern and schematics of graphene and hBN lattices, each rotated 21.8° and 23.0° from the horizon. (**H**) SEM image of triangular WS_2 domains grown on SC-hBN film. The right top and bottom insets show the SEM image of as-grown single-crystal monolayer WS_2 film with a scale bar of 100 μm and the corresponding LEED pattern image with (11$\bar{2}$0) and (10$\bar{1}$0) planes of monolayer WS_2.

Meanwhile, the ex situ growth of SC-WS_2 film on SC-hBN film is performed. To synthesize SC-WS_2, SC-hBN film is coated with a W precursor, and the growth of WS_2 film is further carried out at 900°C under Ar, H_2, and ammonium sulfide atmosphere (supplementary materials and methods). The aligned triangular WS_2 domains are clearly observed (Fig. 3H), and large-scale monolayer WS_2 film successfully proceeds at a prolonged growth time (right-top inset of Fig. 3H). This is markedly distinct from a previous report that both on-top and inverse triangular WS_2 domains are mixed on bare Au, leading to polycrystalline WS_2 film (figs. S19A and S20) (*23*). Therefore, SC-hBN film plays a crucial role to attain homogeneous orientation of the triangular WS_2 domains. The synthesis of such homogeneous triangular WS_2 domains is further confirmed by Raman spectroscopy, photoluminescence, and scanning tunneling electron microscopy (fig. S21). All triangular WS_2 domains have similar aligned orientations within ±1.33° (fig. S19, C and D), and a single set of six hexagonal dots of SC-WS_2 film (LEED) is clearly observed (Fig. 3H), revealing that the large-area monolayer WS_2 film is indeed a single crystal. The growth of MoS_2 domains with similar orientations is also achieved (fig. S22), further supporting universal growth of SC-hBN film as a substrate for the transition metal dichalcogenides. In contrast with SC-Gr-hBN heterostructure film, the presence of hBN after growth of WS_2 film is not detected, indicating that the hBN film might have been substituted or etched away during the growth of WS_2 film. Further study is required to understand the growth mechanism for SC-WS_2 film on SC-hBN film.

We further demonstrate that the wafer-scale SC-hBN film can serve as a protecting layer against metal oxidation and a gas-diffusion barrier for water vapor transmission (*24*, *25*). Cu foil is chosen as a test metal, which is easily oxidized in air. For the oxidation test, hBN film is transferred onto Cu foil (supplementary materials and methods). For comparison, PC-hBN film synthesized on solid Au substrate is used (fig. S9). The Cu surface covered by SC-hBN film is not noticeably changed after the oxidation test at 300°C in air, whereas both PC-hBN–covered and bare Cu surfaces are severely oxidized (Fig. 4, A, F, K and B, G, L), indicative of the change

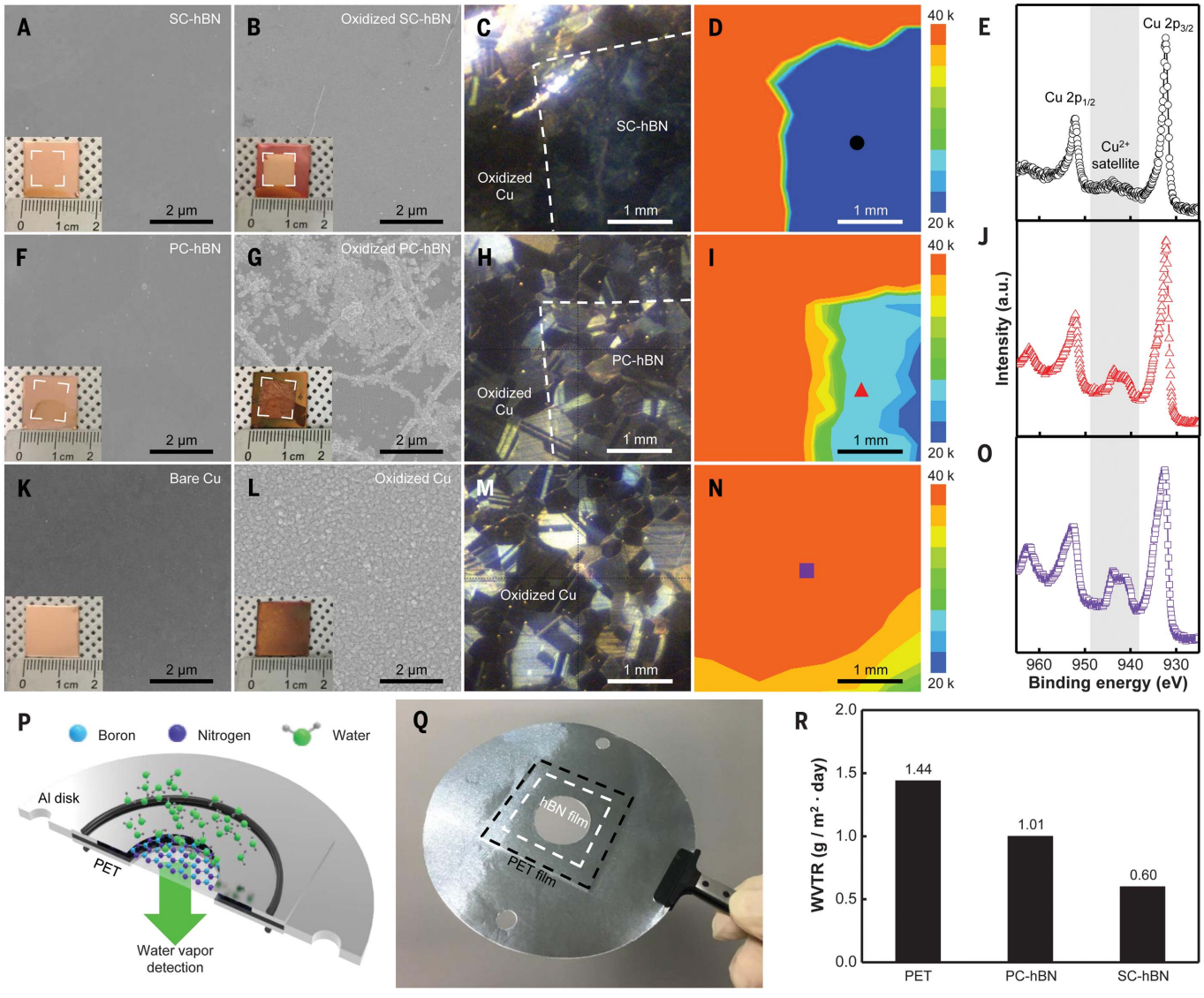

Fig. 4. Protecting layer against Cu oxidation and water vapor barrier applications of wafer-scale SC-hBN film. SEM images of SC-hBN–, PC-hBN–covered, and bare Cu foils before (**A**, **F**, and **K**) and after (**B**, **G**, and **L**) oxidation in air at 300°C for 1 hour. Optical (**C**, **H**, and **M**) and corresponding XPS (**D**, **I**, and **N**) mapping images of SC-hBN, PC-hBN, and bare Cu samples after oxidation. (**E**, **J**, and **O**) Representative Cu 2p core level spectra from the circle, triangle, and square symbols from (D), (I), and (N). The peaks near 952.2 and 932.3 eV in the spectra are assigned to Cu $2p_{1/2}$ and Cu $2p_{3/2}$, respectively. (**P** and **Q**) Schematic and photograph for the WVTR measurement. (**R**) WVTR values of PET, PC-hBN, and SC-hBN samples.

of color from orange to dark orange in each photograph. Some regions of PC-hBN–covered Cu surface withstand oxidation because of the presence of hBN grains (Fig. 4G), but O_2 or H_2O gases easily permeate through the structural defects such as grain boundary or point defect, leading to Cu oxidation. For quantitative analysis of Cu oxidation, the samples are characterized by optical microscope and corresponding XPS mapping for the Cu^{2+} satellite peak near 943 eV in Cu 2p core-level spectra, related to CuO (Fig. 4, C, H, M and D, I, N) (*26*). The XPS mapping image for the SC-hBN sample is quite uniform with low intensity of the CuO peak (Fig. 4D), whereas PC-hBN and bare Cu samples show prominent CuO peaks (Fig. 4, I and N). The representative CuO peak in Cu 2p core-level spectra for SC-hBN sample is negligible, whereas it appears developed for both PC-hBN and bare Cu samples (Fig. 4, E, J, and O). For gas-diffusion barrier application, water vapor transmission rate (WVTR) measurement is carried out for hBN film transferred onto polyethylene terephthalate (PET) film (Fig. 4, P to R and supplementary materials and methods). The WVTR values of PC-hBN and SC-hBN monolayer films are obtained to be 1.01 and 0.60 g/m^2·day, respectively, which are 30% and 58% less than that of PET (1.44 g/m^2·day). The SC-hBN monolayer film outperforms the PC-hBN monolayer film by approximately a factor of 2. The obtained WVTR value is comparable to that of monolayer polycrystalline graphene film (*27*), but it is envisaged to be further improved after optimization of the transfer technique. The wafer-scale SC-hBN film does not have any grain boundary, resulting in a water vapor barrier and the complete protection against Cu oxidation.

In summary, we have synthesized SC-hBN film by means of self-collimation between self-regulated circular hBN grains without a grain boundary. The key step is the facile rotation of circular hBN grains on the liquid Au substrate, regulated by attractive electrostatic interaction between B and N atoms at the perimeter of each grain that eventually leads to the single-crystal growth of hBN film on a wafer scale. The SC-hBN film serves as a promising substrate for the single-crystal growth of the graphene/hBN heterostructure and WS_2 film on a wafer scale. Our strategy for the synthesis of SC-hBN film opens a new horizon for the single-crystal growth of other 2D materials and their heterostructures on a wafer scale.

REFERENCES AND NOTES

1. J. Xue *et al.*, *Nat. Mater.* **10**, 282–285 (2011).
2. J. Wang *et al.*, *Adv. Mater.* **28**, 8302–8308 (2016).
3. S. K. Jang, J. Youn, Y. J. Song, S. Lee, *Sci. Rep.* **6**, 30449 (2016).
4. H.-S. Ra, A.-Y. Lee, D.-H. Kwak, M.-H. Jeong, J.-S. Lee, *ACS Appl. Mater. Interfaces* **10**, 925–932 (2018).
5. B. Amorim, J. Schiefele, F. Sols, F. Guinea, *Phys. Rev. B* **86**, 125448 (2012).
6. L. Britnell *et al.*, *Nano Lett.* **12**, 1707–1710 (2012).
7. R. W. Cahn, *ASM Handbook: Binary Alloy Phase Diagrams–Second edition* (ASM International, 1990).
8. H. Okamoto, T. B. Massalski, "Au-B (Gold-Boron)" in *Binary Alloy Phase Diagrams* (ASM International, ed. 2, 1990), pp. 340–342.
9. L. Tan *et al.*, *Adv. Electron. Mater.* **1**, 1500223 (2015).
10. K. K. Kim *et al.*, *Nano Lett.* **12**, 161–166 (2012).
11. Y. Liu, S. Bhowmick, B. I. Yakobson, *Nano Lett.* **11**, 3113–3116 (2011).
12. X. Fu, R. Zhang, *Nanoscale* **9**, 6734–6740 (2017).
13. Y. Xue *et al.*, *Nanoscale Res. Lett.* **8**, 49 (2013).
14. N. Alem *et al.*, *Phys. Rev. B* **80**, 155425 (2009).
15. M. L. Odlyzko, K. A. Mkhoyan, *Microsc. Microanal.* **18**, 558–567 (2012).
16. L. Wirtz, A. Rubio, R. A. de la Concha, A. Loiseau, *Phys. Rev. B* **68**, 045425 (2003).
17. J.-H. Park *et al.*, *ACS Nano* **8**, 8520–8528 (2014).
18. E. A. Soares, G. S. Leatherman, R. D. Diehl, M. A. Van Hove, *Surf. Sci.* **468**, 129–136 (2000).
19. R. C. Paul *et al.*, "Study of uniaxial tensile properties of hexagonal boron nitride nanoribbons" in *TENCON 2017 – 2017 IEEE Region 10 Conference* (IEEE, 2017), p. 2783.
20. A. Falin *et al.*, *Nat. Commun.* **8**, 15815 (2017).
21. W. Yang *et al.*, *Nat. Mater.* **12**, 792–797 (2013).
22. S. Tang *et al.*, *Sci. Rep.* **3**, 2666 (2013).
23. F. Hanke, J. Björk, *Phys. Rev. B* **87**, 235422 (2013).
24. Z. Liu *et al.*, *Nat. Commun.* **4**, 2541 (2013).
25. J. Meyer *et al.*, *Adv. Mater.* **21**, 1845–1849 (2009).
26. S. Poulston, P. M. Parlett, P. Stone, M. Bowker, *Surf. Interface Anal.* **24**, 811–820 (1996).
27. T. H. Seo *et al.*, *Sci. Rep.* **6**, 24143 (2016).

ACKNOWLEDGMENTS

We thank H. Jung in the Department of Chemistry at Dongguk University for the discussion about the self-collimation of hBN grains. **Funding:** S.M.K. acknowledges support by the Basic Science Research Program through the National Research Foundation of Korea (NRF) funded by the Ministry of Science, ICT and Future Planning (2018R1A2B2002859), and the Korea Institute of Science and Technology (KIST) Institutional Program. K.K.K. acknowledges support by the Basic Science Research Program through the National Research Foundation of Korea (NRF) funded by the Ministry of Science, ICT and Future Planning (2015R1C1A1A02037083) and (2018R1A2B2002302). Y.-M.K. acknowledges support by the Institute for Basic Science (IBS-R011-D1) and Creative Materials Discovery Program (NRF-2015M3D1A1070672) through the NRF grant. S.J.Y. and Y.H.L. acknowledge support by the Institute for Basic Science (IBS-R011-D1). **Author contributions:** J.S.L., K.K.K., and S.M.K. designed and developed this work. S.H.C. and S.B. performed the growth of SC-WS_2. S.J.Y. performed Raman and PL measurements. Y.-M.K. and Y.I.K. performed TEM measurements. J.H.P. performed POM measurement. B.G.S. performed the LEED measurement. H.K. performed the experiments of the protecting layer and WVTR measurement. S.H.L. and Y.H.L. guided and analyzed the work. J.S.L, K.K.K., Y.H.L., and S.M.K. wrote the manuscript. All authors participated in the manuscript review. **Competing interests:** The authors have no competing interests. **Data and materials availability:** All data are available in the main text or the supplementary materials.

SUPPLEMENTARY MATERIALS

www.sciencemag.org/content/362/6416/817/suppl/DC1
Materials and Methods
Figs. S1 to S22
Table S1
References (*28*–*39*)

30 May 2018; accepted 3 October 2018
10.1126/science.aau2132

Science

Wafer-scale single-crystal hexagonal boron nitride film via self-collimated grain formation

Joo Song Lee, Soo Ho Choi, Seok Joon Yun, Yong In Kim, Stephen Boandoh, Ji-Hoon Park, Bong Gyu Shin, Hayoung Ko, Seung Hee Lee, Young-Min Kim, Young Hee Lee, Ki Kang Kim and Soo Min Kim

Science **362** (6416), 817-821.
DOI: 10.1126/science.aau2132

Wafer-scale hBN crystalline films

Although wafer-scale polycrystalline films of insulating hexagonal boron nitride (hBN) can be grown, the grain boundaries can cause both scattering or pinning of charge carriers in adjacent conducting layers that impair device performance. Lee *et al.* grew wafer-scale single-crystal films of hBN by feeding the precursors into molten gold films on tungsten substrates. The low solubility of boron and nitrogen in gold caused micrometer-scale grains of hBN to form that coalesced into single crystals. These films in turn supported the growth of epitaxial wafer-scale films of graphene and tungsten disulfide.

Science, this issue p. 817